Optimization Methodology of Polar Direct-Drive Illumination for the National Ignition Facility

D.E.M. Barlow, A. Colaïtis, D. Viala, M.J. Rosenberg, I. Igumenshchev, V. Goncharov, L. Ceurvorst , P.B. Radha, W. Theobald, R.S. Craxton, M.J.V. Streeter, R.H.H. Scott, K. Glize, T. Chapman, and J. Mathiaud

Published version information

Citation: D.E.M. Barlow et al., Optimization Methodology of Polar Direct-Drive Illumination for the National Ignition Facility, Phys. Rev. Lett. **133**, 175101

DOI: https://doi.org/10.1103/PhysRevLett.133.175101

A New Optimization Methodology for Polar Direct Drive Illuminations at the National Ignition Facility

D.E.M. Barlow,[1] A. Colaïtis,[1,2] D. Viala,[1] M. J. Rosenberg,[2] I. Igumenshchev,[2] V. Goncharov,[2] L. Ceurvorst,[2] P. B. Radha,[2] W. Theobald,[2] R. S. Craxton,[2] M.J.V. Streeter,[3] R. H. H. Scott,[4] K. Glize,[4] T. Chapman,[5] and J. Mathiaud[1]

[1)]*CELIA, Université de Bordeaux, Talence 33400, France*

[2)]*Laboratory for Laser Energetics, University of Rochester, Rochester, New York 14623-1299, USA*

[3)]*School of Mathematics and Physics, Queen's University Belfast, Belfast BT7 1NN, United Kingdom*

[4)]*Central Laser Facility, STFC Rutherford Appleton Laboratory, Harwell Oxford, OX11 0QX, United Kingdom*

[5)]*Lawrence Livermore National Laboratory, Livermore, California 94550, USA*

(*Electronic mail: Duncan.Barlow@u-bordeaux.fr)

(Dated: 30 January 2025)

Improved laser illumination uniformity drives shocks and implosions to create more extreme high energy density environments. Predominantly, the geometry of experiments that can be performed is dictated by the layout of beams at laser facilities, limiting inter-facility and multiscale investigations. This Letter presents the first automated, algorithmic approach for generating illumination configurations for high energy density experiments. The method is demonstrated in comparison to a polar direct drive solid target experiment at the National Ignition Facility. The new illumination configuration is simulated to create greater than $\times 3$ higher peak pressure and almost $\times 2$ higher density by maintaining better shock uniformity. The optimization process is performed with reduced computational expense and isotropic plasma profiles, while accounting for the impact of cross-beam energy transfer.

The highest energy laser facilities in the world, the National Ignition Facility (NIF) [1] and Laser Mega-joule (LMJ)[2], are configured with beam ports in the polar regions of the target chamber, for indirect drive inertial confinement fusion (ICF) [3]. The laser energy is incident on the inside of a cylindrical target, where it is converted to x-rays. The x-rays drive an implosion capsule to achieve ignition conditions[4]. The thermal x-ray bath helps to maintain uniform drive throughout the implosion, which is one of the most significant challenges in ICF[5]. Using indirect drive, the NIF recently achieved thermonuclear ignition[6]. To move into the regime of energy production, fusion energy output must be increased, which requires coupling more laser energy to the target. Direct drive (DD)[7] achieves higher laser-to-target coupling, but with stringent conditions on laser drive uniformity. DD facilities are now capable of attaining $\sigma < 2\%$ deviations in drive symmetry required for high performance implosions[8]. However, their laser energy is too small to probe ignition conditions[9,10].

Polar direct drive (PDD) is used to carry out DD experiments at the mega-joule laser facilities [11–15]. The configurations are numerous and varied, but repointing of the laser beams toward the target equator is often used to distribute energy more uniformly. Due to the large laser energies available, PDD has proven to be a useful technique for exploring high energy density physics[16,17], laser-plasma instabilities (LPI)[18–20], hydrodynamic scaling[10,16,21–23] and reliable neutron production [14,15,24]. However, high performance ICF implosions are currently beyond the reach of PDD at the NIF due to several technical challenges, including laser imprint, the lack of a DD cryogenic target positioner, and issues maintaining uniform drive. Instead of gas-filled implosion capsules, solid plastic targets (often doped or deuterated) can provide an easy-to-diagnose platform for laser-target coupling experiments in PDD[17,20,25] and their illumination geometries are still relevant for implosion targets.

Cross-beam energy transfer (CBET) is an LPI that significantly modifies laser coupling and drive distribution for indirect drive[26], and DD[27], including PDD[18,21]. It is a type of stimulated Brillouin scattering due to resonance between two laser waves and an ion-acoustic wave in the plasma. It is also the most important LPI for drive uniformity at the intensities $10^{14} < I < 10^{15}\mathrm{W/cm^2}$ and laser wavelength $\lambda = 351\mathrm{nm}$, which are currently the focus of DD. CBET is one of the few LPI that can be effectively modelled with ray-tracing while coupled to a radiation-hydrodynamic code[26–30] due to the agreement between linear theory and experiments[31,32]. Despite this, it is still one of the most intensive procedures, increasing 3D radiation-hydrodynamic simulation expense by about $\times 5$ and limiting the number that can be run for optimization.

The repointing of the beams towards the equator, often used in PDD, leads to a changing distribution of energy absorption over time due to the expanding plasma and increasing prevalence of CBET. At early times, the plasma has not had time to expand and laser energy is deposited near the critical surface without significant CBET. This period is important as the target is most susceptible to imprint of drive asymmetries from the laser. If the laser is maintained, steady state ablation occurs between the critical surface and the ablation front, which helps to smooth drive asymmetries. Inverse bremsstrahlung deposits energy along the refracting beam's path through the plasma. Laser light travelling directly up the density gradient deposits energy at higher densities, driving the target more efficiently than light which is incident at an oblique angle[33,34]. This geometric effect is then exacerbated by CBET, which transfers energy primarily from high energy incoming beams

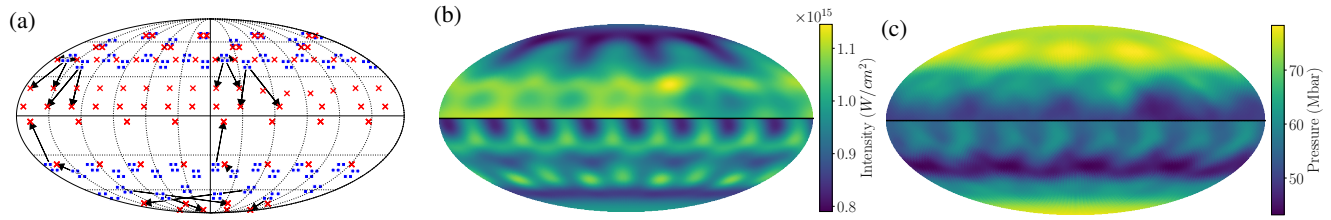

FIG. 1: (a) Mollweide projections showing the NIF target chamber beam locations (blue squares) linked with black arrows to the beam pointing intersections with a 1100 μm radius target (red crosses). The layouts are symmetric about the equator and so half is shown of: (top) A common PDD approach, used in N190204-003 and (bottom) the “Optimized Config" (OC) generated with the method presented in this Letter. In (b) and (c) Mollweide projections each show the target illuminated with N190204-003 (top) and OC (bottom). (b) Intensity on the surface of a target for an illumination without an ablation plasma. (c) An approximation of ablation pressure using Equation 2, simulated with the plasma generated at 4ns through the laser pulse, including the impact of CBET.

to refracted outgoing beams. Both these effects reduce drive, especially at the equator. The propagation of obliquely incident laser beams through a time-varying plasma leads to time dependent drive uniformity, hence the methods used for optimizing conventional DD[35–37] will not adequately optimize PDD. To account for time dependent drive uniformity, some PDD configurations optimize by iteratively changing the beam configuration within a multidimensional radiation-hydrodynamic simulations with CBET modelling capabilities[24,38–40]. Several of these PDD configurations have been tested on solid targets at the NIF and so can provide a benchmark.

The method presented in this Letter is an algorithmic approach for creating PDD illuminations at the NIF. The optimization method uses similar tools to previous attempts including state-of-the-art inverse ray-tracing with the effects of CBET (Ifriit)[41]. However, several key approximations are made which enable new configurations to be tested without running expensive radiation-hydrodynamic codes for each iteration, leading to $\sim \times 1000$ reduction in computational expense. In addition, the optimization of inputs is automated via a numerical method, not a human expert. The whole process requires two 3D radiation-hydrodynamic simulations, an initial simulation to generate the plasma conditions and a final simulation to test the outcome of the optimization. In this Letter, these simulations are performed using the coupled ASTER-Ifriit code[29,42], which is one of several state-of-the-art codes capable of reproducing key experimental features[8]. The method presented starts from randomly generated configurations (within set bounds) and uses isotropic plasma conditions so it does not rely on prior optimizations, highlighting its applicability to new experimental platforms or laser facilities which do not have NIF PDD’s wealth of experimental/numerical data. Beyond the methodology, 3D simulations indicate that the configuration presented in this Letter results in improved drive and convergence symmetry relative to the comparison PDD method, indicating its applicability for future experiments.

The NIF has 192 laser beams arranged into groups of 4, called “quads", as shown in Figure 1a. Each quad enters through a different port on the target chamber, and they have independent beam pointing and power balance [1,43]. The quads are arranged into groups at equal angles from the poles: $\theta_p = 23.5°$, $30.0°$, $44.5°$, and $50.0°$, which are described as “cones". The top and bottom hemisphere of the chamber are symmetric, with 4 cones in each. Each pair of cones (one in the top and bottom) have the same laser spot; however, the laser spot shape and size varies between different pairs. There are other parameters such as quad splitting, wavelength detuning and time varying power balance which were kept at fixed values for this optimization[18,24,39,40].

N190204-003 is a solid target NIF experiment designed to study energy coupling for DD at megajoule scales[17,25] and is used as a benchmark in this letter. N190204-003 uses a PDD illumination, shown in Figure 1a, designed accounting for the impact of CBET[38]. The target was 1000μm radius of deuterated plastic (CD at $1.08 g/cm^3$) surrounded by 100μm of plastic (CH at $1.05 g/cm^3$). The laser pulse was 4.5ns in total, with a two stage ramp up to a peak power of 156TW at 3.5ns[25]. Gated x-ray images[44] of shock ingress were taken from $6-8$ns with peak pressure predicted to occur at 11.7ns[25].

Several approximations were chosen to create a fast and efficient method for the evaluation of laser configurations/illuminations. Each ansatz is discussed below but validated by the overall success of the method. The approximations are: (1) a configuration can be evaluated using snapshots of the plasma at different times, (2) angularly uniform plasma profiles can be used to evaluate 3D beam configurations, (3) uniform pressure at the ablation front leads to uniform drive, (4) plasma conditions from simulating one configuration can be used to evaluate another. The first approximation is typical of finite difference methods, however there is a trade-off between time resolution and accuracy. The second and third assumptions are based on the spherical symmetry of the plasma. The fourth approximation requires that the plasma conditions for each laser configuration evolve in a similar manner. Approximations 2, 3 and 4 are acceptable since it is only the most uniform illuminations that are of interest. These approximations may create false negatives where non-uniform drive generates an anisotropic plasma, which leads to uniform drive. The evaluation of these is not considered

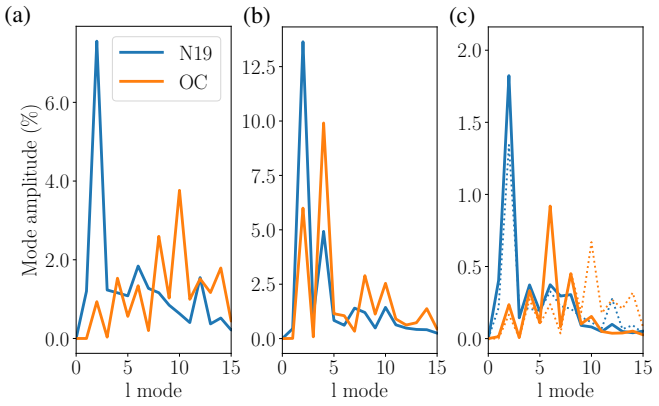

FIG. 2: N190204-003 (N19, blue) and Optimized Config (OC, orange) spherical harmonics "l modes" for: (a) illuminations without an ablation plasma, related to Figure 1b; (b) ablation pressures from Equation 2 generated with plasma and CBET, related to Figure 1c; and (c) target areal densities at $\approx$ 9ns. Mode amplitudes are given as a percentage of the mean. The dotted lines in (c) are a combination of (a) and (b) in quadrature.

here and, although possible, may prove challenging to sustain with dynamic plasma conditions. False positives, illuminations that perform well in uniform plasma conditions but themselves generate anisotropic plasmas with a significant impact on drive uniformity, are evaluated with the use of 3D rad-hydro simulations with CBET, where the efficiency is gained by running fewer of these expensive evaluations (only 2 for this optimization process which considered >500 illumination configurations).

In order to optimize the beam configurations, we must define a fitness function to provide a metric for comparison. Here we propose:

$$f = 10\ \exp\left(-\left(\frac{\sigma_1^2}{9}+\frac{\sigma_2^2}{18}\right)^{1/2}\right)\times\left(\frac{\langle P_{abl}\rangle}{50\text{Mbar}}\right)^2, \quad (1)$$

where σ_1 is the standard deviation of target surface intensity for an illumination with no plasma (Figures 1b and 2a) and σ_2 is the standard deviation of the ablation pressure (Figures 1c and 2b), both as percentages of the mean and only including perturbations up to spherical harmonic $l = 30$. $\langle P_{abl}\rangle$ is the angular mean of the ablation pressure. The method for calculating ablation pressure used in this Letter is presented in the appendix, where P_{abl} is defined by Equation 2. σ_2 and $\langle P_{abl}\rangle$ are evaluated in an angular averaged plasma, which is a snapshot at 4.0ns from a 3D radiation-hydrodynamic simulation of N190204-003. When optimizing, the same plasma is used for all evaluations, but the configuration of lasers is changed to maximize $f(\sigma_i, \langle P_{abl}\rangle)$. In doing so, ablation pressure is increased while reducing deviations from uniform drive. Equation 1 is not unique and is unlikely to be an optimal fitness function, where the numerical factors were adjusted empirically but initially set as a goal for each respective term such that $f \approx 1$ upon successful optimization.

Cone	Polar angle (°)	Offset angle (°)	Defocus (mm)	Power (%)
1	6.36	52.02	8.22	66.26
2	14.95	160.75	9.07	66.26
3	52.48	-12.14	4.67	95.05
4	85.62	6.90	6.83	82.88

TABLE I: OC parameters for each of the 4 cones in a hemisphere. The polar angle is the pointing angle from the pole, offset angle is an azimuthal offset from the port location, defocus changes the best focus along the beam propagation direction and power balance is quoted as a percent of 4TW/quad.

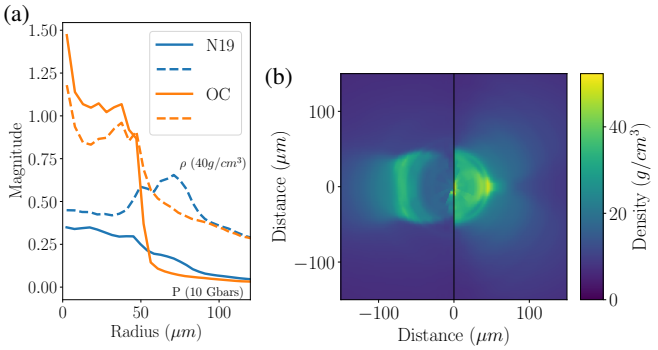

FIG. 3: (a) Shows pressure (normalized to 10Gbars) as solid lines and density (normalized to $40g/cm^3$) as dashed lines for N190204-003 (11.75ns) and the OC (12.20ns) close to peak pressure in each simulation. (b) Shows a density slice at peak compression for N19 (left) and the OC (right).

The NIF has thousands of parameters specifying each configuration, so inherent symmetries are used to reduce this number to 16. Parameters are held constant within a cone, and its symmetric pair. For each of the 4 cones within a hemisphere, 4 parameters are varied: power $[p]$, defocus $[d]$, and 2D target surface pointing $[r_s, \varphi_s]$. The power balance is bounded $2 < p < 4$TW/quad. The pointings and defocus are described relative to the location on the target surface closest to the chamber port of origin for the respective quad $[\theta_p, \phi_p]$. The location of best focus is varied along the direction of laser propagation using defocus, $0 < d < 10$mm with $d = 0.0$mm being on the target surface. The defocus model used is symmetric either side of the target surface and defocusing results in varying the spot size on target, see appendix for more details. Independently, the pointings are varied to cover the half of the target visible from the port. This can be described by circular polar coordinates $0 < r_s < r_t$ and $-180° < \varphi_s < +180°$ (r_t is the target radius which, for N190204-003 is $r_t = 1100\mu$m), $r_s = 0$ is at $[\theta_p, \phi_p]$ for each quad. This is a description of the bounds, but an area preserving map from a square to disk was used to generate the pointings without a polar bias[45]. The 4 parameters are varied between the 4 cones, giving a total of 16 independent parameters.

A genetic algorithm [46] and a coordinate descent/ascent method[47] were used to maximize Equation 1 by varying the 16 input parameters. The methods are derivative-free meaning that exact local gradients are not available. The resultant

Configuration	σ_1	σ_2	$\langle P_{abl} \rangle$	f	@t_3				@t_4				N_{beams}	E_{li}	f_{abs}
					t_3	σ_3	p_3	ρ_3	t_4	σ_4	p_4	ρ_4			
N190204-003	8.56%	14.83%	63.5Mbar	0.18	9.00ns	2.01%	95Mbars	4gcc	11.8ns	16.35%	2.9Gbar	19gcc	184	397kJ	82%
Optimized Config	6.03%	12.56%	56.0Mbar	0.35	9.20ns	1.13%	80Mbars	4gcc	12.2ns	5.56%	11Gbar	37gcc	192	408kJ	77%

TABLE II: List of simulation diagnostics values. σ_1, σ_2 and $\langle P_{abl} \rangle$ are the variables in Equation 1 used to define the fitness function f. Time t_3 is after the end of the laser pulse, during shock ingress, and is chosen to match the shock radius in each simulation. At time t_3, σ_3 is the standard deviation in target areal density, p_3 is the pressure and ρ_3 is the density both at the shock front. p_4 and ρ_4 are given at t_4 which is the time of peak pressure in each simulation, and are averaged over the region where pressure is greater than half the peak pressure. N_{beams} is the number of beams used in the simulation, E_{li} is the incident laser energy and f_{abs} is the absorbed laser energy percentage.

configuration, referred to as the "Optimized Config" (OC), does not represent a maximum in the search space, however it exceeded the fitness, according to Equation 1, of the PDD configuration used in N190204-003 within a certain allocation of compute time ($<$ 2MCPU hours). The parameters for the OC are given in Table I, where the angles are given in terms of target surface coordinates $[\theta, \phi]$. A quantitative comparison of N190204-003 and the OC is displayed in Table II. The OC was found within 550 searched configurations, which consisted of 185 genetic algorithm evaluations and 365 coordinate descent evaluations. It can take $> 10,000$ evaluations for the method to settle at a (local/global) maximum, determined by the optimizations of σ_1 alone. This Letter does not focus on the search procedure, which is an active area of research within mathematics/computer science, but the overall method used to evaluate illumination configurations.

Figure 1a shows the difference in pointing between N190204-003, and the OC. N190204-003 features "quad-splitting" where the pointings for the 4 beams within a single quad differ, and time varying power balances, where each cone's fraction of the total laser energy varies over time, whereas the OC does not. The OC does have independent defocus for each of the cones, whereas $d = 10$mm is used for all cones in N190204-003. The overall complexity of each configuration is similar, and it is likely that they each present a similar level of challenge to recreate experimentally. Additional details for recreating the illumination configurations are given in the appendix.

Figure 1b shows the energy deposition for two configurations illuminating a 1100μm radius target without a plasma. This is similar to the absorption that occurs at the start of the laser pulse ($<$ 0.5ns). The spherical modes for the two illuminations are given in Figure 2a and σ_1 is given in Table II. N190204-003 has a larger mode 2, which leads to it having a larger overall σ_1. Figure 1c is created by illuminating the angularly averaged plasma conditions from a 3D radiation-hydrodynamic simulation of N190204-003 at 4ns. The OC has a smaller mode 2, which can also be seen in Figure 2b, but a larger mode 4. Table II shows that the OC has a smaller overall σ_2 but also a predicted reduction in $\langle P_{abl} \rangle$ when compared to N190204-003.

Once an illumination configuration is selected for maximizing Equation 1, it is evaluated with a full 3D radiation-hydrodynamics simulation. The cone power values given in Table I have been rescaled so that the incident laser energy (E_{li}) matches the experimentally requested laser pulse of N190204-003. The rescaling increased drive asymmetry of OC from $\sigma_2 = 8.83\%$ due to the non-linear effects of CBET. N190204-003 uses the delivered pulse while OC is simulated with the requested pulse, leading to different E_{li} in Table II. Despite this, N190204-003 couples more energy to the target.

Figure 2c shows the modes in areal density for simulation of the N190204-003 configuration at 9.0ns and the OC at 9.2ns. The times are chosen so that the shock radius matches, as can be seen in appendix Figure 4b. Figure 2c also shows dotted lines, which are a combination of the modes from Figures 2a and 2b in quadrature, with the same weightings used in Equation 1. It shows the strengths and weaknesses of the initial approximations. In Figure 2c, the difference between the solid and the dashed lines for the modes $\gtrsim 8$ is likely due to the Bell-Plesset effect[48]. The OC also features a mode 6 in the areal density, which is not seen in the two snapshots. This is caused by a combination of the inhomogeneous plasma and temporal resolution, which are lacking within the optimization procedure but present in the 3D radiation hydrodynamic simulations. The matching of modes is not a requirement for the method to work; however, the similarity is evidence that reinforces the initial assumptions. Additional analysis of the shock shape during ingress is included in the appendix alongside Figure 4.

Figure 3a shows angular averaged profiles of density and pressure for N190204-003 and the OC for the time at which peak pressure occurs. Table II shows that N190204-003 features an earlier peak pressure at, $t_4 = 11.75$ns due to the larger amount of energy absorbed (f_{abs}). But, σ_4 is approximately $\times 3$ that of the OC, resulting in N190204-003's lower p_4 and ρ_4 despite coupling more energy to the target. This is highlighted by the difference in symmetry displayed in Figure 3b. In this deuterated solid target experiment, higher density and pressure at shock convergence could create the conditions necessary for fusion, giving an x-ray flash which is a useful diagnostic but was not observed in N190204-003.

The simulated drive uniformity demonstrated in this paper is an important step, however, more is required to use PDD to drive an implosion to ignition at the NIF. It has not been demonstrated that both σ_1 and σ_2 can be reduced below $\approx 2\%$ required for a high performance implosion[8]. Using a similar method, it may be possible to achieve the requisite $\sigma_i < 2\%$ for all times if the power balance was varied between the snapshots. In addition, it is likely that for implosions, more snapshots will need to be considered. Time varying power balance would add a new parameter per cone per snapshot, and

so principal component analysis[49] could be used to reduce the parameter space.

This methodology has a range of applications for any multi-beam compression facility, such as, multistage-zooming[50], particle generation[51,52], backlighting[38], or generation of magnetic fields[53]. Similar to PDD, in each case there is an area of the target which is challenging to provide uniform ablation pressure, either due to beams that must be removed from the main drive or blocked by experimental apparatus. The optimization of the beam configuration is relatively simple for a surface illumination, but much more difficult for imploding targets with expanding plasmas and CBET. This is the first algorithmic approach for optimizing both simultaneously.

Demonstrated in this letter is a new, efficient, algorithmic approach to creating illumination configurations for PDD solid targets. This alone is a critical development, as previously methods for development have required many hours from a human expert, alongside numerous radiation-hydrodynamic simulations. Beyond this the illumination configuration is novel, practical and results in higher peak pressure and density when simulated by 3D radiation-hydrodynamics. The method can be modified for implosion targets and the process is not limited to spherical PDD, but could provide efficient optimization where illumination uniformity is important, regardless of target/chamber geometry. It could also be vital for DD as future designs are expected to require many beams per port to balance drive uniformity[54,55], against chamber efficiency. DD with multiple beams per port can no longer rely on traditional techniques and will require iterative optimization such as the method presented here to achieve the necessary drive uniformity.

ACKNOWLEDGMENTS

We would like to acknowledge support and funding from the CNRS, CEA, and Université de Bordeaux including the staff of CELIA. This work has been carried out within the framework of the EUROfusion Consortium, funded by the European Union via the Euratom Research and Training Programme (Grant Agreement No 101052200 - EUROfusion). Views and opinions expressed are however those of the author(s) only and do not necessarily reflect those of the European Union or the European Commission. Neither the European Union nor the European Commission can be held responsible for them. The involved teams have operated within the framework of the Enabling Research Project: ENR-IFE.01.CEA 'Advancing shock ignition for direct-drive inertial fusion'. This work was granted access to the HPC resources of TGCC under the Allocation Nos. 2023-A0140514117 made by GENCI. We would like to acknowledge the help of Philippe Nicolai in accessing GENCI. M.J.V.S. acknowledges support from the Royal Society URF-R1221874. This material is partially based upon work supported by the Department of Energy [National Nuclear Security Administration] University of Rochester "National Inertial Confinement Fusion Program" under Award Number(s) DE-NA0004144. Disclaimer: This report was partially prepared as an account of work sponsored by an agency of the United States Government. Neither the United States Government nor any agency thereof, nor any of their employees, makes any warranty, express or implied, or assumes any legal liability or responsibility for the accuracy, completeness, or usefulness of any information, apparatus, product, or process disclosed, or represents that its use would not infringe privately owned rights. Reference herein to any specific commercial product, process, or service by trade name, trademark, manufacturer, or otherwise does not necessarily constitute or imply its endorsement, recommendation, or favoring by the United States Government or any agency thereof. The views and opinions of authors expressed herein do not necessarily state or reflect those of the United States Government or any agency thereof.

The code and data used for optimization are available via an MIT license from Github: https://github.com/DuncanBarlow/PDDOptimisation, release tag: v0.1.0-alpha. For access to the other codes used please contact the author. The data will also be uploaded to a repository linked to the journal.

Appendix on approximating ablation pressure. Laser energy deposited at a lower density results in lower P_{abl}, ablation pressure[33]. Here P_{abl} is generated from a weighted radial sum of the absorbed intensity,

$$P_{abl} = 24.7\ \text{Mbar}\left(\frac{\mathrm{F(I_r)}}{10^{14}[\mathrm{W/cm^2}]}\right)^{2/3}, \tag{2a}$$

$$F(I_r) = \frac{1}{R_{351}^2 n_{351}^{2/3}} \sum_{r=0}^{\infty} r^2 n_r^{2/3} I_r, \tag{2b}$$

where R_{351} and n_{351} are the critical radius and electron number density for wavelength $\lambda = 351$nm and I_r is the laser intensity absorbed ($\mathrm{W/cm^2}$) at radius r with electron number density n_r. I_r is defined over a volume with radial extent Δr and solid angle Ω, such that the total power deposited is $P = \sum_\Omega \Omega \sum_{r=0}^{\infty} r^2 I_r$. The r^2 in Equation 2b is applied to convert intensity to units $\mathrm{W/sr}$. Equation 2a is based on Ref. 33. $n_r^{2/3}$ is an empirical weighting chosen to match pressure and asymmetries observed in several 3D radiation-hydrodynamic simulations. P_{abl} is calculated for all angular directions to produce an ablation pressure map, as seen in Figure 1c.

Appendix on the defocus model. The pointings shown for the OC on the bottom of Figure 1 display a red cross per beam. It is assumed that the defocused beams overlap exactly at this point on the original target surface at a radius of 1100μm (the point is defined quantitatively in Table I). The NIF optics defocus the entire quad and so the beams within the quad must be repointed after defocusing to achieve this overlap experimentally. The paraxial wave solver, pF3D[56], was used to characterise the beam spot shapes up to a defocus of 10mm. The beam spots produced by pF3D were fitted empirically by modifying the $1/e$ radius of the super Gaussian in mm,

$$\sigma_\alpha = \sigma_{0,\alpha}(1 + d\beta), \tag{3}$$

where the subscript α denotes the x or y axis of the beam, d corresponds to the defocus in mm and the fitting factor

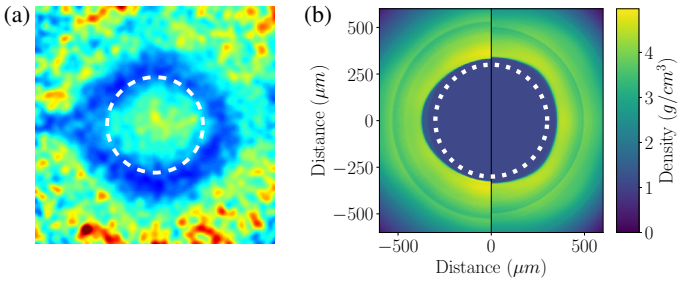

FIG. 4: (a) A backlit gated x-ray image of N190204-003 experiment at 7.7ns which indicates path integrated density via detector response with arbitrary units. The elliptical shape of the ingoing shock is visible as the dark blue region. (b) Density slice from 3D simulation of N190204-003 at 9.0ns (left) and OC at 9.2ns (right). The overlaid white dashed circles are visual guides.

$\beta = \{0.30/50,\ 0.40/50,\ 0.80/50,\ 0.95/50\}$ was determined for each of the NIF's cones, $\theta_p = \{23.5°, 30.0°, 44.5°, 50.0°\}$. A good fit was achieved using the same β for the x and y axes within each beam. In the most extreme case, this is a $\approx 20\%$ correction to beam radius. Ifriit models the beams as planar waves, where Equation 3 was used to match the beam spot at the initial target surface. Away from this surface, Ifriit's model deviates from the true beam envelope. This is acceptable since the beam-plasma interaction happens over a few mm while the beam envelope varies on the order of tens of mm as seen in Equation 3. When combined, the overlap of beams on the target surface, the defocus model, and the planar wave model used in Ifriit, our system is symmetric to defocus into or out of the target plane, however care must be taken when replicated experimentally where this is not the case.

Appendix on creating the illumination configurations. The OC has a small deviation from top/bottom illumination symmetry, not shown in Figure 1. This is due to the chamber ports having a rotational symmetry but, the pointings were selected to point in the same azimuthal direction in each hemisphere. The symmetry was broken to reduce the overlap between reflected and incoming beams travelling in opposite directions at the equator with the aim of reducing CBET however the impact is minimal due to the small offset angle for cone 4 seen in Table I.

Figure 1a shows that for N190204-003 two of the quads were used for an x-ray backlighter and some of the surrounding beams have modified powers and pointings to mitigate the reduced uniformity. When N190204-003 is compared to the illumination with all 192 beams on target and without the modified pointings/power balance, only a minor modification in illumination uniformity is observed (σ_i changes by $< 1\%$), indicating that the mitigation was effective.

Appendix on shock shape during ingress. Figure 4a shows a flat-field corrected, backlit gated x-ray image[44] of the N190204-003 shock at 7.73ns[17,25]. The white dashed circle has similar radius to the minor radius of the shock (at the pole) but is smaller than the major radius (at the equator). The simulation of N190204-003 shown in Figure 4b has a similar shape but at a later time, 9.0ns. Figure 4b shows the improved shape that is achieved when using the OC for illuminating the target. This is reinforced by comparing σ_3 in Table II.

N190204-003 uses power balance to compensate for the late stage, drive efficiency reduction in the equatorial region. This leads to modal "swing" whereby early stage drive is biased towards the equator and late stage drive is greater in the poles (see the top of Figure 1 b and c). The OC configuration uses power balance and greater offset on the polar cones to mimic the oblique angles required to get energy to the equator. This reduces the modal swing and as such the mode 2 is consistently smaller throughout shock ingress.

[1] C. Haynam, P. Wegner, J. Auerbach, M. Bowers, S. Dixit, G. Erbert, G. Heestand, M. Henesian, M. Hermann, K. Jancaitis, *et al.*, "National ignition facility laser performance status," Applied optics **46**, 3276–3303 (2007).

[2] J. Miquel, C. Lion, and P. Vivini, "The laser mega-joule: Lmj & petal status and program overview," in *Journal of Physics: Conference Series*, Vol. 688 (IOP Publishing, 2016) p. 012067.

[3] S. Atzeni and J. Meyer-ter Vehn, *The physics of inertial fusion: beam plasma interaction, hydrodynamics, hot dense matter*, Vol. 125 (OUP Oxford, 2004).

[4] J. D. Lindl, P. Amendt, R. L. Berger, S. G. Glendinning, S. H. Glenzer, S. W. Haan, R. L. Kauffman, O. L. Landen, and L. J. Suter, "The physics basis for ignition using indirect-drive targets on the national ignition facility," Physics of plasmas **11**, 339–491 (2004).

[5] C. Li, F. Séguin, J. Frenje, R. Petrasso, J. Delettrez, P. McKenty, T. Sangster, R. Keck, J. Soures, F. Marshall, *et al.*, "Effects of nonuniform illumination on implosion asymmetry in direct-drive inertial confinement fusion," Physical review letters **92**, 205001 (2004).

[6] H. Abu-Shawareb, R. Acree, P. Adams, J. Adams, B. Addis, R. Aden, P. Adrian, B. Afeyan, M. Aggleton, L. Aghaian, *et al.*, "Lawson criterion for ignition exceeded in an inertial fusion experiment," Physical review letters **129**, 075001 (2022).

[7] R. Craxton, K. Anderson, T. Boehly, V. Goncharov, D. Harding, J. Knauer, R. McCrory, P. McKenty, D. Meyerhofer, J. Myatt, *et al.*, "Direct-drive inertial confinement fusion: A review," Physics of Plasmas **22** (2015).

[8] A. Colaïtis, D. Turnbull, I. Igumenschev, D. Edgell, R. Shah, O. Mannion, C. Stoeckl, D. Jacob-Perkins, A. Shvydky, R. Janezic, *et al.*, "3d simulations capture the persistent low-mode asymmetries evident in laser-direct-drive implosions on omega," Physical Review Letters **129**, 095001 (2022).

[9] T. Boehly, D. Brown, R. Craxton, R. Keck, J. Knauer, J. Kelly, T. Kessler, S. Kumpan, S. Loucks, S. Letzring, *et al.*, "Initial performance results of the omega laser system," Optics communications **133**, 495–506 (1997).

[10] R. Nora, R. Betti, K. Anderson, A. Shvydky, A. Bose, K. Woo, A. Christopherson, J. Marozas, T. Collins, P. Radha, *et al.*, "Theory of hydro-equivalent ignition for inertial fusion and its applications to omega and the national ignition facility," Physics of Plasmas **21** (2014).

[11] S. Skupsky, J. Marozas, R. Craxton, R. Betti, T. Collins, J. Delettrez, V. Goncharov, P. McKenty, P. Radha, T. Boehly, *et al.*, "Polar direct drive on the national ignition facility," Physics of Plasmas **11**, 2763–2770 (2004).

[12] J. Marozas, F. Marshall, R. Craxton, I. Igumenshchev, S. Skupsky, M. Bonino, T. Collins, R. Epstein, V. Y. Glebov, D. Jacobs-Perkins, *et al.*, "Polar-direct-drive simulations and experiments," Physics of plasmas **13** (2006).

[13] B. Canaud, F. Garaude, C. Clique, N. Lecler, A. Masson, R. Quach, and J. Van der Vliet, "High-gain direct-drive laser fusion with indirect drive beam layout of laser mégajoule," Nuclear fusion **47**, 1652 (2007).

[14] A. Cok, R. Craxton, and P. McKenty, "Polar-drive designs for optimizing neutron yields on the national ignition facility," Physics of Plasmas **15** (2008).

[15] C. Yeamans, G. Kemp, Z. Walters, H. Whitley, P. McKenty, E. Garcia, Y. Yang, R. Craxton, and B. Blue, "High yield polar direct drive fusion neutron sources at the national ignition facility," Nuclear Fusion **61**, 046031 (2021).

[16] S. Regan, V. Goncharov, T. Sangster, E. Campbell, R. Betti, K. Anderson,

T. Bernat, A. Bose, T. Boehly, M. Bonino, *et al.*, "The national direct-drive program: Omega to the national ignition facility," Fusion Science and Technology **73**, 89–97 (2018).

[17]L. Ceurvorst, W. Theobald, M. Rosenberg, P. Radha, C. Stoeckl, R. Betti, K. Anderson, J. Marozas, V. Goncharov, E. Campbell, *et al.*, "Development of an x-ray radiography platform to study laser-direct-drive energy coupling at the national ignition facility," Review of Scientific Instruments **93** (2022).

[18]J. Marozas, M. Hohenberger, M. Rosenberg, D. Turnbull, T. Collins, P. Radha, P. McKenty, J. Zuegel, F. Marshall, S. Regan, *et al.*, "First observation of cross-beam energy transfer mitigation for direct-drive inertial confinement fusion implosions using wavelength detuning at the national ignition facility," Physical review letters **120**, 085001 (2018).

[19]A. Solodov, M. Rosenberg, M. Stoeckl, A. Christopherson, R. Betti, P. Radha, C. Stoeckl, M. Hohenberger, B. Bachmann, R. Epstein, *et al.*, "Hot-electron preheat and mitigation in polar-direct-drive experiments at the national ignition facility," Physical Review E **106**, 055204 (2022).

[20]D. Barlow, T. Goffrey, K. Bennett, R. Scott, K. Glize, W. Theobald, K. Anderson, A. Solodov, M. Rosenberg, M. Hohenberger, *et al.*, "Role of hot electrons in shock ignition constrained by experiment at the national ignition facility," Physics of Plasmas **29** (2022).

[21]T. J. Murphy, N. S. Krasheninnikova, G. Kyrala, P. A. Bradley, J. A. Baumgaertel, J. Cobble, P. Hakel, S. C. Hsu, J. L. Kline, D. Montgomery, *et al.*, "Laser irradiance scaling in polar direct drive implosions on the national ignition facility," Physics of Plasmas **22** (2015).

[22]E. Campbell, T. Sangster, V. Goncharov, J. Zuegel, S. Morse, C. Sorce, G. Collins, M. Wei, R. Betti, S. Regan, *et al.*, "Direct-drive laser fusion: status, plans and future," Philosophical Transactions of the Royal Society A **379**, 20200011 (2021).

[23]M. Rosenberg, A. Solodov, C. Stoeckl, M. Hohenberger, R. Bahukutumbi, W. Theobald, D. Edgell, T. Filkins, R. Betti, F. Marshall, *et al.*, "Hot electron preheat in hydrodynamically scaled direct-drive inertial confinement fusion implosions on the nif and omega," Physics of Plasmas **30** (2023).

[24]A. Zylstra, C. Yeamans, S. Le Pape, A. MacKinnon, M. Hohenberger, D. Fittinghoff, H. Herrmann, Y. Kim, P. Radha, P. McKenty, *et al.*, "Enhanced direct-drive implosion performance on nif with wavelength separation," Physics of Plasmas **27** (2020).

[25]D. Viala, A. Colaïtis, D. Barlow, L. Ceurvorst, W. Theobald, I. Igumenshchev, R. Bahukutumbi, M. Rosenberg, K. Anderson, R. Scott, and D. Batani, "Role of cross-beam energy transfer in spherical strong shock polar direct drive experiments at the national ignition facility," In submission.

[26]P. Michel, L. Divol, E. Williams, S. Weber, C. Thomas, D. Callahan, S. Haan, J. Salmonson, S. Dixit, D. Hinkel, *et al.*, "Tuning the implosion symmetry of icf targets via controlled crossed-beam energy transfer," Physical review letters **102**, 025004 (2009).

[27]I. Igumenshchev, D. Edgell, V. Goncharov, J. Delettrez, A. Maximov, J. Myatt, W. Seka, A. Shvydky, S. Skupsky, and C. Stoeckl, "Crossed-beam energy transfer in implosion experiments on omega," Physics of Plasmas **17** (2010).

[28]D. Marion, A. Debayle, P.-E. Masson-Laborde, P. Loiseau, and M. Casanova, "Modeling crossed-beam energy transfer for inertial confinement fusion," Physics of Plasmas **23** (2016).

[29]A. Colaïtis, I. Igumenshchev, J. Mathiaud, and V. Goncharov, "Inverse ray tracing on icosahedral tetrahedron grids for non-linear laser plasma interaction coupled to 3d radiation hydrodynamics," Journal of Computational Physics **443**, 110537 (2021).

[30]R. Follett, A. Colaïtis, D. Turnbull, D. Froula, and J. Palastro, "Validation of ray-based cross-beam energy transfer models," Physics of Plasmas **29** (2022).

[31]D. Turnbull, A. Colaïtis, A. M. Hansen, A. L. Milder, J. P. Palastro, J. Katz, C. Dorrer, B. E. Kruschwitz, D. J. Strozzi, and D. H. Froula, "Impact of the langdon effect on crossed-beam energy transfer," Nature Physics **16**, 181–185 (2020).

[32]A. Hansen, K. Nguyen, D. Turnbull, B. Albright, R. Follett, R. Huff, J. Katz, D. Mastrosimone, A. Milder, L. Yin, *et al.*, "Cross-beam energy transfer saturation by ion heating," Physical Review Letters **126**, 075002 (2021).

[33]W. M. Manheimer, D. Colombant, and J. Gardner, "Steady-state planar ablative flow," The Physics of Fluids **25**, 1644–1652 (1982).

[34]B. Scheiner and M. Schmitt, "The role of incidence angle in the laser ablation of a planar target," Physics of Plasmas **26** (2019).

[35]M. Murakami, "Irradiation system based on dodecahedron for inertial confinement fusion," Applied physics letters **66**, 1587–1589 (1995).

[36]M. Murakami, N. Sarukura, H. Azechi, M. Temporal, and A. Schmitt, "Optimization of irradiation configuration in laser fusion utilizing self-organizing electrodynamic system," Physics of Plasmas **17** (2010).

[37]A. Shvydky, W. Trickey, A. Maximov, I. Igumenshchev, P. McKenty, and V. Goncharov, "Optimization of irradiation configuration using spherical t-designs for laser-direct-drive inertial confinement fusion," Nuclear Fusion **63**, 014004 (2022).

[38]M. Hohenberger, P. Radha, J. Myatt, S. LePape, J. Marozas, F. Marshall, D. Michel, S. Regan, W. Seka, A. Shvydky, *et al.*, "Polar-direct-drive experiments on the national ignition facility," Physics of Plasmas **22** (2015).

[39]T. Collins and J. Marozas, "Mitigation of cross-beam energy transfer in ignition-scale polar-direct-drive target designs for the national ignition facility," Physics of Plasmas **25** (2018).

[40]J. Marozas, M. Hohenberger, M. Rosenberg, D. Turnbull, T. Collins, P. Radha, P. McKenty, J. Zuegel, F. Marshall, S. Regan, *et al.*, "Wavelength-detuning cross-beam energy transfer mitigation scheme for direct drive: Modeling and evidence from national ignition facility implosions," Physics of Plasmas **25** (2018).

[41]A. Colaïtis, R. Follett, J. Palastro, I. Igumenschev, and V. Goncharov, "Adaptive inverse ray-tracing for accurate and efficient modeling of cross beam energy transfer in hydrodynamics simulations," Physics of Plasmas **26** (2019).

[42]I. Igumenshchev, V. Goncharov, F. Marshall, J. Knauer, E. Campbell, C. Forrest, D. Froula, V. Y. Glebov, R. McCrory, S. Regan, *et al.*, "Three-dimensional modeling of direct-drive cryogenic implosions on omega," Physics of Plasmas **23** (2016).

[43]C. Keane, "National ignition facility user guide," Tech. Rep. (Lawrence Livermore National Lab.(LLNL), Livermore, CA (United States), 2014).

[44]G. Kyrala, S. Dixit, S. Glenzer, D. Kalantar, D. Bradley, N. Izumi, N. Meezan, O. Landen, D. Callahan, S. Weber, *et al.*, "Measuring symmetry of implosions in cryogenic hohlraums at the nif using gated x-ray detectors," Review of Scientific Instruments **81**, 10E316 (2010).

[45]P. Shirley and K. Chiu, "A low distortion map between disk and square," Journal of graphics tools **2**, 45–52 (1997).

[46]A. F. Gad, "Pygad: An intuitive genetic algorithm python library," arXiv preprint arXiv:2106.06158 (2021).

[47]S. J. Wright, "Coordinate descent algorithms," Mathematical programming **151**, 3–34 (2015).

[48]R. Epstein, "On the bell–plesset effects: the effects of uniform compression and geometrical convergence on the classical rayleigh–taylor instability," Physics of plasmas **11**, 5114–5124 (2004).

[49]R. Bro and A. K. Smilde, "Principal component analysis," Analytical methods **6**, 2812–2831 (2014).

[50]I. Igumenshchev, D. Froula, D. Edgell, V. Goncharov, T. Kessler, F. Marshall, R. McCrory, P. McKenty, D. Meyerhofer, D. Michel, *et al.*, "Laser-beam zooming to mitigate crossed-beam energy losses in direct-drive implosions," Physical Review Letters **110**, 145001 (2013).

[51]M. Tabak, D. Hinkel, S. Atzeni, E. M. Campbell, and K. Tanaka, "Fast ignition: Overview and background," Fusion science and technology **49**, 254–277 (2006).

[52]J. Fernández, B. Albright, F. N. Beg, M. E. Foord, B. M. Hegelich, J. Honrubia, M. Roth, R. B. Stephens, and L. Yin, "Fast ignition with laser-driven proton and ion beams," Nuclear fusion **54**, 054006 (2014).

[53]C. Walsh, A. Crilly, and J. Chittenden, "Magnetized directly-driven icf capsules: Increased instability growth from non-uniform laser drive," Nuclear Fusion **60**, 106006 (2020).

[54]A. Colaïtis, R. K. Follett, C. Dorrer, A. G. Seaton, D. Viala, I. Igumenshchev, D. Turnbull, V. Goncharov, and D. H. Froula, "Exploration of cross-beam energy transfer mitigation constraints for designing an ignition-scale direct-drive inertial confinement fusion driver," Physics of Plasmas **30** (2023).

[55]D. Eimerl, E. M. Campbell, W. F. Krupke, J. Zweiback, W. Kruer, J. Marozas, J. Zuegel, J. Myatt, J. Kelly, D. Froula, *et al.*, "Stardriver: a flexible laser driver for inertial confinement fusion and high energy density physics," Journal of Fusion Energy **33**, 476–488 (2014).

[56]C. H. Still, R. Berger, A. Langdon, D. Hinkel, L. Suter, and E. Williams, "Filamentation and forward brillouin scatter of entire smoothed and aberrated laser beams," Physics of Plasmas **7**, 2023–2032 (2000).